10th Conference on
Photonic Technologies LANE 2018

Industrial Paper

Influence of laser parameter on weld bead shape and process stability of laser welded steel sheets

Marc Schiry[a*], Peter Plapper[a]

[a] *University of Luxembourg, L-1359 Luxembourg, Luxembourg*

Abstract

Laser butt-welding of dissimilar heat sensitive materials is one of the most challenging tasks. Significant differences in melting and transition temperatures are typical and occur frequently. Therefore, accurate control of the temperature profile at the interface of the weld is essential. In this paper, the influence of the laser parameter power and velocity, as well as laser spot diameter on the laser process were investigated. It is shown that the beam diameter has a significant impact on the weld bead formation. Further variation of the type of shielding gas showed an effect on the bead geometry depending on the used laser spot diameter. Spectroscopic process observations showed a significant impact of the spot diameter and shielding gas on the energy input and the efficiency of the laser process. A homogeneous damping effect of the laser radiation was obtained by using the larger fiber diameter accompanied with a higher overall intensity of process radiation.

Keywords: weld bead shape; process stability; laser welding dissimilar materials; laser welding steel sheets; spectroscopy

1. Introduction

Laser welding of dissimilar materials has received high attention for many applications. Especially the beneficial combination of lightweight and high strength lead to the intensified research activities. Due to the precise heat input, laser welding is a promising technology for welding heat sensitive and dissimilar materials.

High quality joints of heat sensitive materials requires defined temperature control at the interface of the welding partners. Unfavorable temperature profiles in dissimilar butt-joints increase the probability of the formation of harmful intermetallic phases or incomplete bonding of the welding partners [1]–[5].

Due to the material specific bulking temperatures, the weld seam border as well as the heat-affected zone (HAZ) correlate with specific temperatures. Variations of the weld seam shapes lead to changes of the temperature profile at the weld interface in the butt-welding configuration. Several researchers investigated the influence of laser parameters like laser power, welding velocity, focal beam position, laser spot diameter etc. on the process stability and the weld bead formation [6]–[10]. Beside the experimental work, manifold papers deal with multidimensional simulations of fluid flow mechanisms inside the melt bath in laser welding processes. By analyzing the mechanism of Marangoni convection, the authors elucidate the impact of the laser conditions on the bead formation [11]–[18]. Therefore, the investigations pointed out that the Marangoni convection is depended on the oxides on the surface of the liquid melt bath. Admission of different shielding gases influences the oxidation reactions and the final weld seam shape. In addition, shielding gas also affects the formation and the size of the induced plume above the keyhole. Spectroscopic analysis of the emitted process radiation showed the impact of shielding gas on the formation of the plume and the stability of the laser welding process [7], [19]–[22].

The aim of this work is to enlighten the dependency of the weld seam shape and the metal plume behavior on the laser parameter power, welding velocity, spot diameter and the interaction of shielding gas with the laser radiation and the melt bath in butt welding processes. Therefore, the presented work provides the missing link between weld bead formation and metal plume behavior. This paper is structured as follows. In chapter 2 the

* Corresponding author. Tel.: +00352-466644-5560; fax: +00352-466644-5560.
E-mail address: marc.schiry@uni.lu

experimental set up is outlined. Chapter 3 shows the results and the discussion. The paper finally ends with a conclusion and a scientific outlook.

2. Experimental set up

The welding experiments have been carried out by using the Yd:YAG disk laser TruDisk 2000 from company TRUMPF. This laser source emits laser radiation with a wavelength of 1030 nm ±10 nm. A scanner optic (PFO 20-2 from TRUMPF) was connected with the laser by a dual core fiber. This dual core fiber had an inner core diameter of 50 µm, while the outer diameter was 200 µm. The scanner optic was equipped with a focal distance of 160 mm. In addition with the back focal length of the collimator of 90 mm, the laser beam had a diameter of 89 µm for the 50 µm-fiber and a diameter of 356 µm in case of the 200 µm-fiber in the focus point. Beside the two different beam diameter, the fiber diameter also results two different Rayleigh-Lengths. For the 50 µm fiber diameter and with the current collimator, a Rayleigh-Length of 1.171 mm occurred. The 200 µm fiber diameter was accompanied with a Rayleigh-Length of 4.682 mm. The focal spot was vertically set in the middle of the sheet metal and remained in this position during the entire experiments.

Three different energy per unit length values have been defined for the welding experiments (E=25 J/mm, E=35 J/mm and E=45 J/mm). In respect to these values, power and welding speed have been changed in three combinations to fulfill these ratios. For welds with 25 J/mm, the power was set to 1500 W and the welding speed to 60 mm/s. A power of 1400 W and a welding speed of 40 mm/s were given for E=35 J/mm. Finally, for E=45 J/mm a power of 900 W and a velocity of 20 mm/s was used.

All welds have been carried out as a bead-on-plate-weld in carbon steel sheets of the grade SAE 6135. The samples had a size of 45x35x1.12 mm. Due to the high energy density on top of the steel sheet, a deep penetration welding process was given. Therefore, the laser beam penetrated the steel sheet completely. Because of the full penetration, 2 shielding gas nozzles have been positioned on both sides of the sample (figure 1).

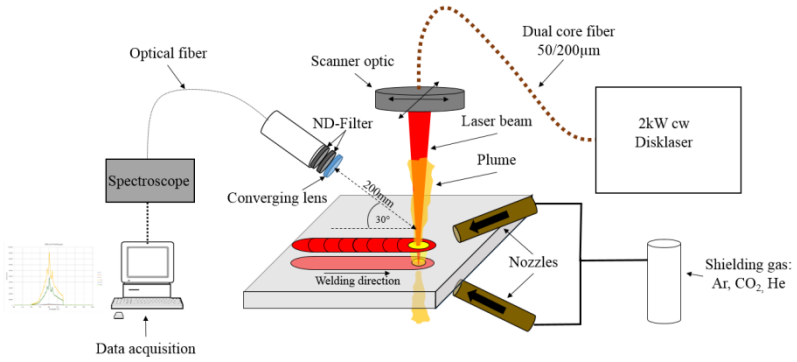

Figure 1. Experimental set up

Argon (99.996 % purity), Helium (99.996 % purity) and CO_2 (99.995 % purity) were used to identify the influence of the type of shielding gas on the welding process. For a sufficient gas supply, the flow rate was set to 21 l/min and kept constant for all experiments. The formation and the behavior of the laser induced metal plume above the keyhole were observed with the spectroscope HR2000+ from company OCEAN-OPTICS. By doing so, the emitted process radiation was focused by a converting lens and coupled into an optical fiber, which guided the light into the spectroscope. The lens was positioned in a distance of 200 mm to focal point of the laser beam on the surface of the steel sheet and oppositional to the welding direction. To avoid an overload signal, the integration time of the spectroscope was set to 1 ms and two neutral density filter (ND-filter) were mounted behind the lens. While the process radiation generated with the 356 µm laser spot had a significant higher intensity, a ND-filter with 5 % and a filter with 10 % permeability were positioned in a row. In case of welds performed with the 89 µm beam diameter, the 5 % ND-filter was sufficient to avoid the overload. Protection of the spectroscope against the high intense laser radiation was realized by using a short pass filter (cut-off wavelength 750 nm) for both fibers. The transmission behavior of this filter was nearly 100 % in the range of 380-740 nm.

Conventional spectroscopic process observation uses the light intensity as quality criteria. By doing so, the result strongly depends on the properties of the optical components and the record parameter (e.g. integration time). To avoid this not reproducible influence on the result, the radiation density was used to classify the spectroscopic results. It is calculated based on the following equation:

$$L = \sum_{\lambda=188nm}^{1090nm} \frac{I(\lambda) \cdot h \cdot D \cdot c}{t_{int} \cdot A_{CCD}} \cdot \frac{1}{\lambda} \left[\frac{W}{m^2}\right]$$

(1)

In this equation, I represents the measured intensity at a particular wavelength, h the Planck constant, D the damping factor of the optical components, c the speed of light, t_{int} the adjusted integration time, A_{CCD} the size of the CCD sensor (5.734 mm²) and λ the wavelength. The resulting radiation density L has the unit power per area.

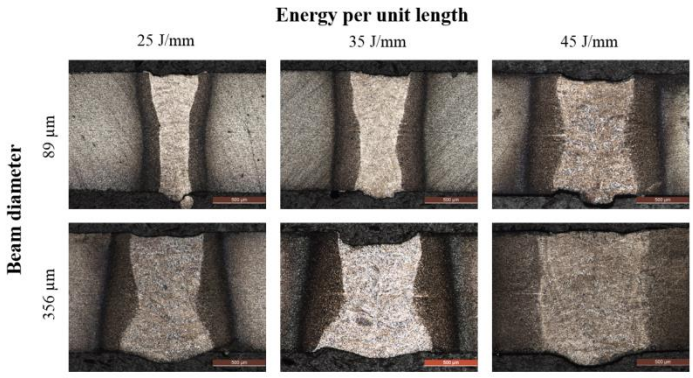

Figure 2. Cross-sections of weld without shielding gas

For the weld seam examination, the welded samples were cut, embedded in a thermoplastic resin, grinded and polished. After the etching with Nital etchant (3 % nitric acid on alcohol base), the microstructure was observed under an optical microscope.

3. Results

3.1 Welding with the beam diameter of 89 µm

Cross-sections of the different weld seams performed without shielding gas are shown in figure 2. Welds produced with E=25 J/mm and the 50 µm- fiber show nearly an I-shape weld bead. An decrease of the welding speed and in addition, an increase in the energy up to 35 J/mm generates an intermediate weld bead shape, which represents a transition of an I-shaped and a X-shaped seam geometry. An ongoing reduction of the welding speed leads to a higher energy and a X-shaped bead profile. The narrowest point of the X is located in the middle of the steel sheet. This correlates with the vertical focal position of the laser beam, which was also positioned in the middle of the sample. However, the significant higher energy density of the 89 µm laser spot causes a minor impact to the bead profile. The same reduced influence can be observed on the process radiation. Increase of the energy values cause a moderate intensification of the process radiation. Only the process radiation measured for welds performed with E=35 J/mm show a slight increased radiation density. Because of the high energy density of the laser beam, the defocusing influence of the metal plume as a function of different power and velocity ratios is less critical (figure 3). However, the type of shielding has a more significant impact on the bead shape and the process radiation.

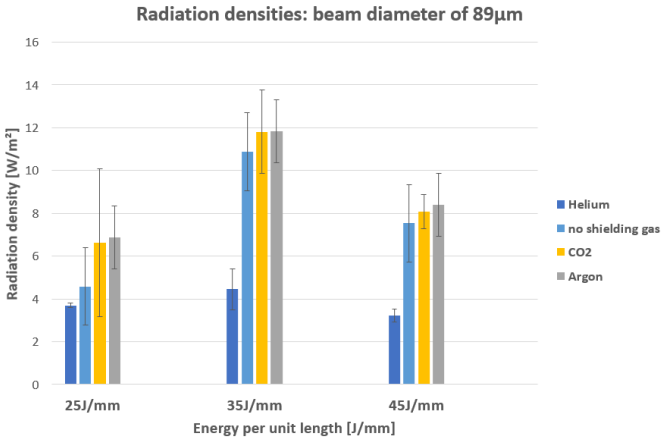

Admission of argon reduces the weld seam width. The resulting bead shape shows a X-shaped geometry. A change of the type of shielding gas from argon to CO_2 and helium results a low influence on the bead formation (figure 4). However, the different shielding gases cause a distinct difference on the surface morphology of the weld seam. Spatter and an inhomogeneous width occurs when welding without any shielding gas. Argon stabilizes the melt flow and generates a smooth surface. Due to the interaction of the oxygen of the CO_2 gas with the liquid melt bath, the seam surface shows clear oxidation products. A homogenous seam surface was obtained with helium potentially as shielding gas. In addition, helium enhances the process stability. Due to the higher heat conductivity, helium cools the metal bath and the metal plume. This leads to a modified melt bath convection and stabilizes the process by reducing the plume temperature and therefore the interaction of laser radiation with the metal gas. In comparison to the welds without shielding gas, CO_2 and Argon reduce the process stability and intensify the process radiation. This can be explained by the flow behaviors and interaction of the metal plume with the shielding gas. Argon and CO_2 have a higher specific mass compared to the air, while helium has a lower one. This difference in the density leads to unequal flow properties. The low amount of metal

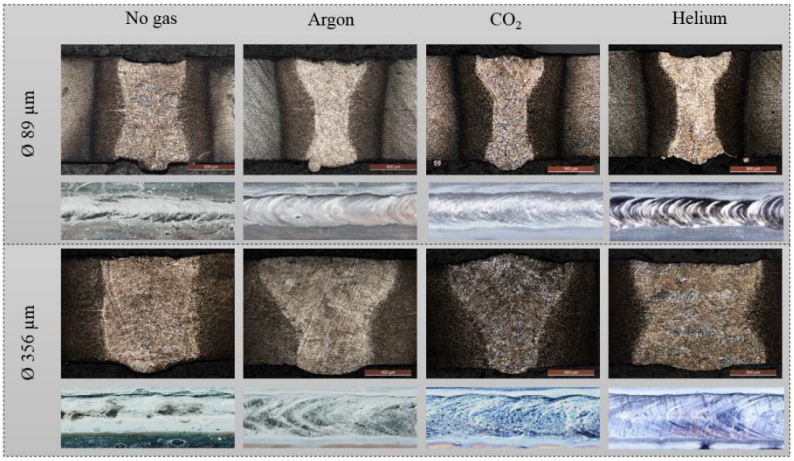

Figure 4. Cross-sections and surfaces of welds with E=45 J/mm

plume interferes with the gas and intensifies the process radiation. However, this increase in the radiation density is quite low compared to the results obtained with the 356 µm beam diameter.

3.2 *Welding with the beam diameter of 356 µm*

In contrast, the seam shapes generated with the 200 µm-fiber show a distinct development in the geometries. Due to the significant lower energy density of laser spot with the 356 µm beam diameter, variations of the energy per unit length values affect the bead shape. Low energy leads to X-shaped weld seams, while lower welding speed and higher energy causes a wide I-shaped profile. Furthermore, the type of shielding as also affects the Marangoni convection and the surface morphology of the weld seam.

As [22] showed, argon potentially interacts with the laser radiation. This interaction leads to defocusing beam caustic and a reduction of the energy in the laser spot. The changed heat input affects the fluid low in the melt bath and finally the bead formation. A X/Y-shaped bead shape is the consequence, where a wide upper width and a narrow lower seam width can be measured. However, a smooth seam surface occur. The radiation density

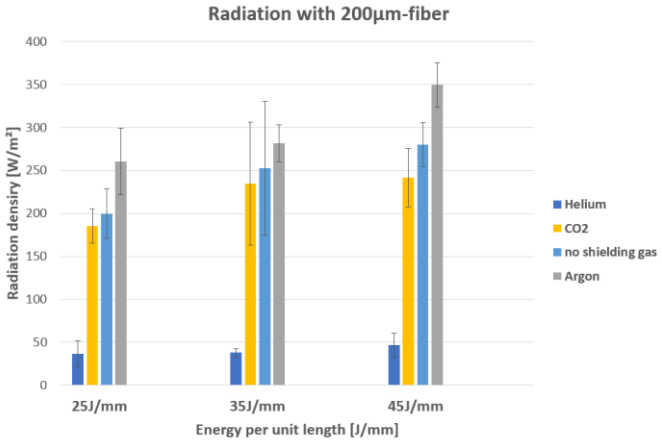

Figure 5. Radiation densities with 356 µm beam diameter

of the emitted process glow is significantly increased by using argon as shielding gas. In contrast, CO_2 reduces the process radiation. In the cross-section, the bead has a predominant V-shaped profile. Comparable to the previous welds, oxidation products are located on the weld seam surface. The lowest process radiation was obtained by using helium. Similar to the welds performed with the smaller beam diameter, a smooth and homogenous seam surface can be achieved with helium. The cooling effect of helium reduces the process radiation and allows a higher energy supply into the keyhole. A wide X-shaped seam geometry is the result.

4. Conclusion

Application of different beam diameters impacts the bead geometry and the process stability. With the same optic, the beam caustic changes under different fiber diameters. An enlarged Rayleigh-Length and spot diameter is the consequence for increased fiber diameters. Therefore, smaller fiber diameters cerate higher energy densities in the focal point. This high energy density leads to narrow weld seams as well as to a less critical damping effect of the laser radiation caused by the initialized metal plume. High welding speed promotes the formation of I-shaped weld seam. The resulting vertical seam boundaries are favorable for welding heat sensitive material. The resulting homogenous vertical temperature profile along the phase transition area liquid / solid allows to obtain defined temperatures at the interface of a butt-welded joint. Lower welding speed leads to X-shaped weld seams, which hinders to ensure a defined temperature profile at the interface with a complete bonding of both welding partners. Shielding gas shows a limited effect to the bead shape. However, helium stabilizes the process by cooling the melt bath and the metal plume. A smooth and homogenous seam surface can be generated.

The same influence of helium on the process stability and the weld surface can be observed for a larger beam diameter. A smooth surface, accompanied with low process radiation is achieved by using helium as shielding gas. Due to the lower energy density in the laser spot, the type of shielding gas affects the bead profile significantly. While argon promotes X/Y-shaped weld seams, CO_2 causes V-shaped bead profiles. In addition, the interaction of laser beam and metal plume can be reduced by using CO_2 shielding gas. Due to the low interaction of helium with the laser radiation, the seam geometry shows a X-shaped appearance. Welds without shielding gas enable wide I-shaped seams. However, welds performed without shielding gas and higher welding speeds lead to X-shaped beads. An I-shaped bead profile only can be produced with higher energy densities and without shielding gas. Unfortunately, these welding conditions are associated with high process radiation and, due to the large seam volume, with slow cooling speeds. Especially for dissimilar material combination of heat sensitive materials, this leads to multiple problems (thermal stresses, distortion, formation of intermetallic phases, etc.). Therefore, these materials should be welded with high laser spot energy densities (small fiber), high welding speed and helium as shielding gas. By doing so, a stable process with a defined temperature profile at the interface can be achieved. Future research activities will focus on the detailed understanding of the interaction mechanisms between shielding gas and the liquid melt bath as well as on the fluid dynamics of the gas. For understanding the complex interaction mechanism, CFD-simulations are needed. Based on the deep understanding, purposeful manipulation of the bead shape should be possible. With the following control of the temperatures at the interface and the heat input, multiple dissimilar heat sensitive materials can be welded in a butt-joint configuration by means of laser welding.

5. References

[1] J. S. At, 1987, “The joining of tungsten carbide hardmetal to steel”, In: Journal of the South African Institute of Mining and Metallurgy, vol. 87, no. 5, pp. 125–135.

[2] M. R. Locatelli, B. J. Dalgleish, K. Nakashima, A. P. Tomsia, and A. M. Glaeser, 1997. “ New approaches to joining ceramics for high-temperature applications”, In: Ceramics International., vol. 23, no. 4, pp. 313–322.

[3] Z. Mohid, M. A. Liman, M. R. A. Rahman, N. H. Rafai, and E. A. Rahim, 2013, “Dissimilar Materials Laser Welding Characteristics of Stainless Steel and Titanium Alloy”, In: Applied Mechanics and Materials, vol. 465–466, pp. 1060–1064.

[4] T. A. Mai and A. C. Spowage, 2004,“Characterisation of dissimilar joints in laser welding of steel-kovar, copper-steel and copper-aluminium”, In: Materials Science and Engineering A, vol. 374, no. 1–2, pp. 224–233.

[5] P. Schmalen and P. Plapper, 2016, “Evaluation of Laser Braze-welded Dissimilar Al-Cu Joints”, In: Physics Procedia, vol. 83, pp. 506–514.

[6] A. El-Bataahgy, 1997,“Effect of laser welding parameters on fusion zone shape and solidification structure of austenitic stainless steels”, In: Journal of Materials Letters, vol. 32, no. August, pp. 155–163.

[7] Y. Kawahito, M. Mizutani, and S. Katayama, 2007, “Elucidation of high-power fibre laser welding phenomena of stainless steel and effect of factors on weld geometry”, In: Journal of Physics D: Applied Physics., vol. 40, no. 19, pp. 5854–5859.

[8] K. Y. Benyounis, A. G. Olabi, and M. S. J. Hashmi, 2005, “Effect of laser welding parameters on the heat input and weld-bead profile”, In: Jornal of Materials Processing Technology, vol. 164–165, pp. 978–985.

[9] K. Manonmani, N. Murugan, and G. Buvanasekaran, 2007,“Effects of process parameters on the bead geometry of laser beam butt welded stainless steel sheets”, In: International Journal of Advanced Manufacturing Technology, vol. 32, no. 11–12, pp. 1125–1133.

[10] A. Ruggiero, L. Tricarico, A. G. Olabi, and K. Y. Benyounis, 2011, “Weld-bead profile and costs optimisation of the CO2 dissimilar laser welding process of low carbon steel and austenitic steel AISI316”, In: Optics and Laser Technology, vol. 43, no. 1, pp. 82–90.

[11] A. Robert and T. Debroy, 2001, “Geometry of laser spot welds from dimensionless numbers”, In: Metallurgical and Materials Transactions B, vol. 32, no. 5, pp. 941–947.

[12] M. Akbari, S. Saedodin, D. Toghraie, R. Shoja-Razavi, and F. Kowsari, 2014, “Experimental and numerical investigation of temperature distribution and melt pool geometry during pulsed laser welding of Ti6Al4V alloy”, In: Optics & Laser Technology, vol. 59, pp. 52–59.

[13] K. Kazemi and J. A. Goldak, 2009, “Numerical simulation of laser full penetration welding”, In: Computational Materials Science, vol. 44, no. 3, pp. 841–849.

[14] H. Du, L. Hu, J. Liu, and X. Hu, 2004, “A study on the metal flow in full penetration laser beam welding for titanium alloy”, In: Computational Materials Science, vol. 29, no. 4, pp. 419–427.

[15] X. Jin, L. Li, and Y. Zhang, 2003, “A heat transfer model for deep penetration laser welding based on an actual keyhole”, In: International Journal of Heat and Mass Transfer, vol. 46, no. 1, pp. 15–22.

[16] R. Rai, S. M. Kelly, R. P. Martukanitz, and T. DebRoy, 2008, “A Convective Heat-Transfer Model for Partial and Full Penetration Keyhole Mode Laser Welding of a Structural Steel”, In: Metallurgical and Materials Transactions A, vol. 39, no. 1, pp. 98–112.

[17] K. Chongbunwatana, 2014, “Simulation of vapour keyhole and weld pool dynamics during laser beam welding”, In: Production Engineering, vol. 8, no. 4, pp. 499–511.

[18] A. P. Mackwood and R. C. Crafer, 2005, “Thermal modelling of laser welding and related processes: a literature review”, In: Optics & Laser Technology, vol. 37, no. 2, pp. 99–115.

[19] P. Sathiya, M. K. Mishra, and B. Shanmugarajan, 2012, “Effect of shielding gases on microstructure and mechanical properties of super austenitic stainless steel by hybrid welding”, In: Materials & Design, vol. 33, no. 1, pp. 203–212.

[20] T. Sibillano, A. Ancona, V. Berardi, E. Schingaro, G. Basile, and P. Mario Lugarà, 2006, “A study of the shielding gas influence on the laser beam welding of AA5083 aluminium alloys by in-process spectroscopic investigation”, In: Optics and Lasers in Engineering, vol. 44, no. 10, pp. 1039–1051.

[21] A. R. Konuk, R. G. K. M. Aarts, A. J. H. in’t Veld, T. Sibillano, D. Rizzi, and A. Ancona, 2011, “Process Control of Stainless Steel Laser Welding using an Optical Spectroscopic Sensor”, In: Physics Procedia, vol. 12, pp. 744–751.

[22] D. H. Abbott and C. E. Albright, 1994, “CO 2 shielding gas effects in laser welding mild steel”, In: Journal of Laser Applications, vol. 6, no. 2, pp. 69–80.